



TESTING AND MODELING OF DIAGONALLY REINFORCED CONCRETE COUPLING BEAMS

D. Naish¹ and J. W. Wallace²

ABSTRACT

An efficient structural system for tall building construction to resist earthquake loads consists of reinforced concrete shear walls connected by diagonally reinforced coupling beams. Construction of coupling beams that satisfy the strength and detailing requirements set forth in ACI 318-05 for diagonally reinforced coupling beams is cumbersome and costly; therefore, ACI 318-08 provides a new detailing option which aims to improve the constructability while maintaining adequate strength and ductility. Seven half-scale specimens were tested to compare the performance of beams constructed utilizing new and old detailing options, to evaluate common modeling approaches, and to assess the impact of reinforced and post-tensioned slabs on the load-deformation response of the beam. Test results indicate that the new detailing approach provides equal, if not improved behavior as compared to the alternative detailing approach, that simple modeling approaches reasonably capture measured force versus deformation behavior, and that including a slab had only a modest impact on strength, stiffness, ductility, and observed damage.

Introduction

Tall building construction is common in metropolitan areas and it has become increasingly important to provide methods of construction that improve both seismic performance and constructability. Reinforced concrete core walls, with coupling beams above openings to accommodate doorways, are an efficient lateral-force-resisting system for tall buildings. When subjected to strong shaking, coupling beams act as fuses and typically undergo large inelastic rotations. Various testing programs have been carried out to assess the load – deformation behavior of coupling beams. Based on investigation of prior studies [(Paulay 1974), (Tassios 1996), (Galano 2000)], the following parameters were deemed particularly important for study: aspect ratio (span to depth ratio), residual capacity/failure, slab inclusion (RC and PT), and detailing of confinement steel.

Use of diagonal reinforcement in coupling beams with clear length to total depth less than four was introduced into ACI 318-95. Providing transverse reinforcement around the diagonal bar bundles, to suppress diagonal bar buckling, as detailed in ACI 318-05 S21.7.7 is difficult where the diagonal groups intersect at the beam mid-span, particularly for shallow beams, as well as at the beam-wall interface due to interference with the wall boundary vertical

¹Graduate Student, Dept. of Civil Engineering, UCLA, Los Angeles, CA 90024

²Professor, Dept. of Civil Engineering, UCLA, Los Angeles, CA 90024

reinforcement. ACI 318-08 S21.9.7 introduced an alternative detailing option, where transverse reinforcement is placed around the beam cross section to provide confinement and suppress buckling, with no transverse reinforcement provided directly around the diagonal bar bundles.

Nonlinear modeling of coupling beams has received increased attention as the use of performance-based design for tall core wall buildings has become more common (Wallace 2007). Modeling parameters for diagonally-reinforced coupling beams were introduced into Table 6-18 of FEMA 356. Of particular interest is the selection of the effective secant bending stiffness at yield $E_c I_{eff}$ and the allowable plastic rotation prior to significant lateral strength degradation. The value used for coupling beam bending stiffness has a significant impact on the system behavior.

Experimental Program

The test beam prototypes were based on two common tall building configurations for residential and office construction. Typical wall openings and story heights produce coupling beams with aspect ratios of approximately 2.4 for residential buildings and 3.33 for office buildings. A coupling beam with cross-section dimensions of 24" x 30" and 24" x 36" reinforced with two bundles of 8-#11 diagonal bars is common for residential and office construction, respectively. Due to geometric and strength constraints of an existing reaction frame, tests were conducted on one-half scale replicas of the prototype beams. Thus the test specimens were 12" x 15" (CB24F and CB24D) and 12" x 18" (CB33F and CB33D) with two bundles of 6-#7 diagonal bars, for the residential and office beams, respectively (Fig.1).

Beams with transverse reinforcement provided around the bundles of diagonal bars (referred to as "Diagonal confinement") were designed according to ACI 318-05 S21.7.7.4, whereas beams with transverse reinforcement provided around the entire beam cross section (referred to as "Full section confinement") were designed according to ACI 318-08 S21.9.7.4(d). Due to maximum spacing requirements, the volumetric ratios of transverse reinforcement provided in both the prototype and test beams exceed that calculated using the requirement for columns (ACI 318-08 21.6.4.4). Three test specimens with aspect ratio of 2.4 were constructed with 4"-thick slabs. One specimen (CB24F-RC) contained a slab reinforced with #3 bars @12" spacing, on the top and bottom in the transverse direction, and on the top only in the longitudinal direction, without post-tensioning strands. Two specimens (CB24F-PT and CB24F-1/2-PT) both contained a similar reinforced-concrete slab, but also were reinforced with 3/8" 7-wire strands post-tensioned to apply 150 psi to the slab in the longitudinal direction. Specimen geometries and material properties are summarized in Table 1. Further details can be found in (Naish 2009).

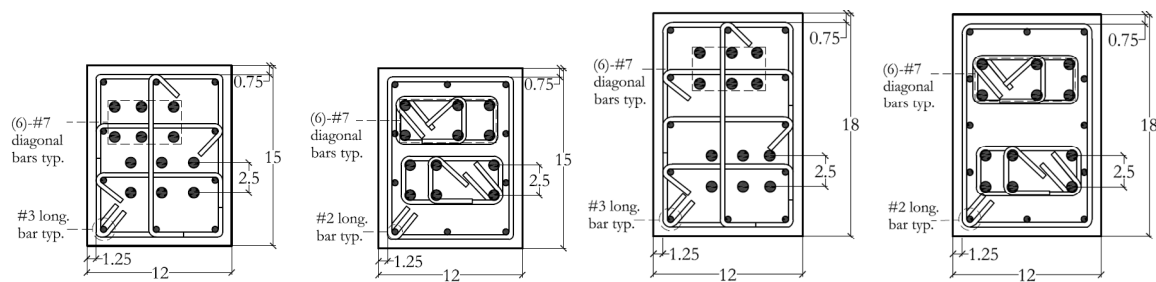


Figure 1. From left to right, beam cross-section for CB24F, CB24D, CB33F, and CB33D. A 4"

slab is included on the top of CB24F-RC, PT, ½-PT, with 36” overhang on each side. Diameter and spacing of hoops and cross ties indicated in Table 1. Diagonal bars embedded 32” into end blocks for 2.4 aspect ratio, and 22” with terminators for 3.33 aspect ratio. (1in = 25.4mm)

The test specimens were each placed in a vertical position with end blocks simulating wall boundary zones at each end, and tested using the setup shown in Fig. 2. The lateral load was applied via a horizontal actuator. Two vertical hydraulic actuators were used to ensure zero rotation at the top of the specimen, while maintaining constant (zero) axial force in the beam. Load-control testing was performed at 0.125, 0.25, 0.50, and 0.75 V_y , where $V_y = 2M_y/l_n$ to ensure that the load-displacement behavior prior to yield was captured. Beyond 0.75 V_y , displacement-control was used in increments of percent chord rotation (θ), defined as the relative lateral displacement over the clear span of the beam (Δ) divided by the beam clear span (l_n). Three cycles were applied at each load increment for load controlled testing, and three cycles were applied in displacement-control at each increment of chord rotation up to 3%. Two cycles were applied at each increment of chord rotation exceeding 3%.

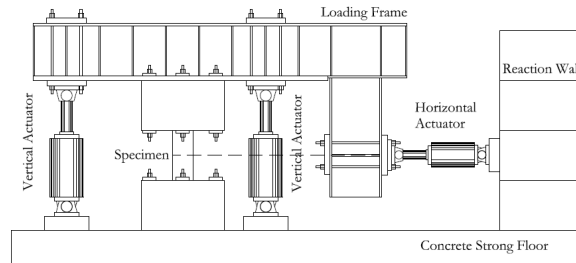


Figure 2. Laboratory test setup.

Table 1. Test matrix and material properties.

Beam	l_n/h type	α [°]	Transverse Reinforcement		f'_c [psi]	f_y [psi]	f_u [psi]	Description
			Full Section	Diagonals				
CB24F	2.4 residential	15.7	#3 @ 3"	N.A.	6800	70000	90000	Full section confinement (ACI 318-08)
CB24D			#2 @ 2.5"	#3 @ 2.5"	6800			Diagonal confinement (ACI 318-05)
CB24F-RC			#3 @ 3"	N.A.	7300			Full section conf. w/ 4" thick RC slab (ACI 318-08)
CB24F-PT			#3 @ 3"	N.A.	7200			Full section conf. w/ 4" thick PT slab (ACI 318-08)
CB24F-1/2-PT			#3 @ 6"	N.A.	7000			Full section conf. (reduced) w/ 4" PT slab (ACI 318-08)
CB33F			3.3 office	12.3	#3 @ 3"			N.A.
CB33D	#2 @ 2.5"	#3 @ 2.5"			6800	Diagonal confinement (ACI 318-05)		

Experimental Results

Detailing

Load-deformation responses of CB24F and CB24D are very similar over the full range of applied rotations (Fig. 3a). Notably, both beams achieve large rotation ($\sim 8\%$) without significant degradation in the lateral load carrying capacity, and the beams achieve shear strengths of 1.25 and 1.17 times the ACI nominal strength (Table 2). The shear strength of CB24D degraded rapidly at around 8% rotation, whereas CB24F degraded more gradually, maintaining a residual shear capacity of $\sim 80\%$ of V_{ave} at a rotation of 10% . V_{ave} is defined as the average shear force resisted by the beam between the yield point and the onset of significant lateral strength degradation. Fig. 2b plots load vs. rotation relations for the 3.33 aspect ratio beams with full section confinement (CB33F) vs. diagonal confinement (CB33D). Similar to the 2.4 aspect ratio beams, Fig. 3b reveals that the beams have similar strength, stiffness, and deformation characteristics. The test results presented in Fig. 3 indicate that the full section confinement option of ACI 318-08 provides equivalent, if not improved performance, compared to confinement around the diagonals per ACI 318-05.

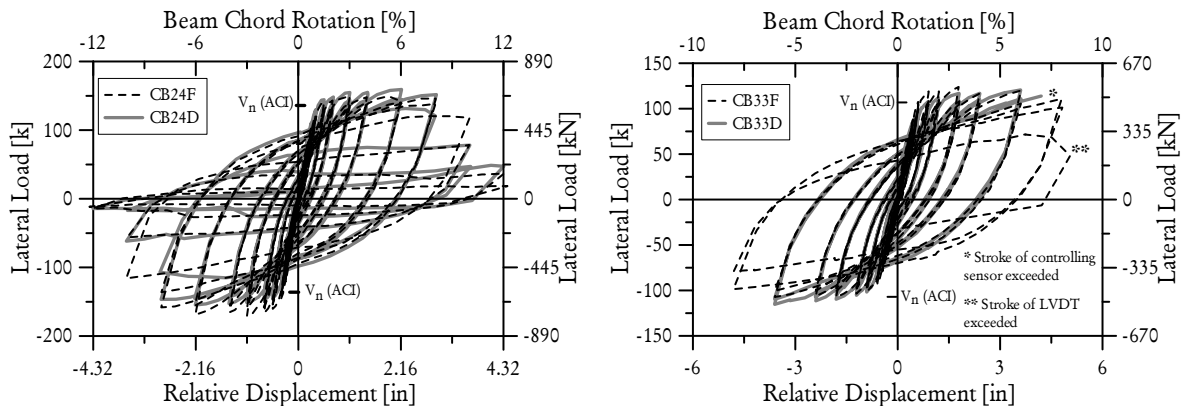


Figure 3. Cyclic load-deformation: (a) CB24F vs. CB24D; (b) CB33F vs. CB33D.

The transverse reinforcement used for CB24F-1/2-PT was one-half that used for CB24F-PT to assess the impact of using less than the code-required transverse reinforcement given that the requirements of S21.6.4 are based on column requirements. Fig. 4 plots load-deformation responses and reveals similar loading and unloading relations up to 3% total rotation, which approximately corresponds to the Collapse Prevention limit state per ASCE 41-06. At higher rotations ($\theta \geq 4\%$), modest strength degradation is observed for CB24F-1/2-PT, whereas the strength of CB24F-PT continues to increase slightly; however, both beams achieve rotations of $\sim 8\%$ before significant lateral strength degradation ($< 0.8V_{ave}$).

The results indicate that the one-half scale coupling beams tested with ACI 318-08 detailing are generally capable of achieving total rotations exceeding 8% , whereas ASCE 41 limits plastic rotation to 3% without strength degradation and 5% with 20% strength degradation. The potential influence of scale on the test results is discussed later. The test results indicate that there is little difference in load-deformation response between CB24F-PT and

CB24F-1/2-PT; therefore, the potential to reduce the quantity of required transverse reinforcement exists, but requires further study since only one beam test was conducted.

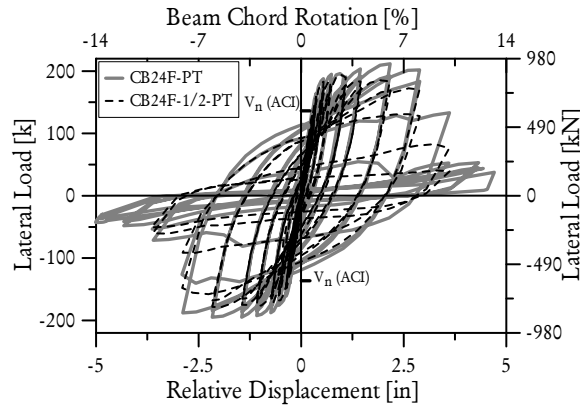


Figure 4. Cyclic load-deformation: CB24F-PT vs. CB24F-1/2-PT.

Slab Influence

Four beams with aspect ratio of 2.4 were tested to systematically assess the impact of a slab on the load-deformation responses. CB24F did not include a slab, whereas CB24F-RC included an RC slab, and CB24F-PT and CB24F-1/2-PT included PT slabs (with 150 psi of prestress). Fig. 5, which directly compares the load-displacement responses of CB24F vs. CB24F-RC, reveals that the slab increases shear strength by 17% (155 k to 181 k); however, this strength increase can be taken into account by considering the increase in nominal moment strength due to the presence of the slab, i.e. slab concrete in compression at the beam-wall interface at one end, and slab tension reinforcement at the beam-wall interface at the other end. The results, summarized in Table 2, indicate that the higher test shear strength observed is primarily due to the increase in nominal moment capacity when a slab is present.

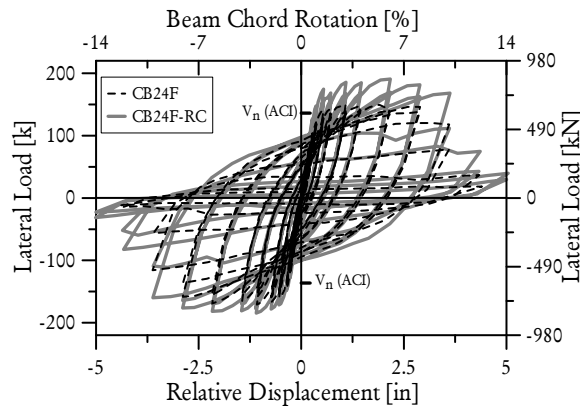


Figure 5. Cyclic load-deformation: CB24F vs. CB24F-RC.

Table 2. Summary of analytical moment and shear capacities, and experimental strength and deformation capacities.

Beam	M_n^+ [in-k]	M_n^- [in-k]	$V@M_n$ [k]	$\frac{V@M_n}{\sqrt{f'_c A_{cv}}}$	$V_n(ACI)$ [k]	$\frac{V_n(ACI)}{\sqrt{f'_c A_{cv}}}$	V_{ave} [k]	$\frac{V_{ave}}{\sqrt{f'_c A_{cv}}}$	V_y [k]	Δ_y [in]	V_{max} [k]	$\Delta@V_{max}$ [in]
CB24F	2850	2850	158.3	10.65	136.3	9.15	154.9	10.40	121.3	0.360	171.0	1.08
CB24D	2850	2850	158.3	10.65	136.3	9.15	150.7	10.12	128.8	0.363	159.2	2.16
CB24F-RC	2890 3550*	2890 3350*	160.6 191.7*	10.45 12.50*	136.3	8.87	181.0	11.77	147.2	0.362	190.8	2.16
CB24F-PT	3160 3960*	3160 3625*	175.6 210.7*	11.45 13.75*	136.3	8.90	198.9	12.98	163.2	0.361	211.8	2.16
CB24F-1/2-PT	3145 3940*	3145 3610*	174.7 209.7*	11.61 13.90*	136.3	9.06	182.4	12.12	158.1	0.365	189.6	1.08
CB33F	3615	3615	120.5	6.77	107.8	6.03	118.3	6.62	107.7	0.600	124.0	1.80
CB33D	3615	3615	120.5	6.77	107.8	6.03	114.7	6.42	95.94	0.601	120.6	3.60

*Calculations consider the impact of the slab concrete and reinforcement on the M- ϕ analysis.
Note: V_{ave} is defined as the average shear force resisted by the beam between the yield point and the onset of significant lateral strength degradation.

Modeling

Elastic analysis approaches require estimation of the effective elastic bending and shear stiffness values. There are several methods available for determination of effective (secant) stiffness values at yield for coupling beams. These methods are summarized and compared to test results in Table 3. The low secant stiffness ratios (I_{eff}/I_g) relative to recommended values might imply that significant damage (cracking, concrete spalling) is required to achieve these ratios. However, photos of beam damage (Fig. 6) do not show significant spalling and diagonal crack widths are limited to 1/32" even at 6% total rotation; damage is concentrated at the beam-wall interface in the form of slip/extension cracks. Of the various approaches, only ASCE 41-06 addressed the impact of slip/extension deformations on the effective yield stiffness. The contribution of slip/extension to the yield rotation is estimated for the beams tested using the approach recommended by Alsiwat and Saatcioglu, where the crack width that develops at the beam-wall interface depends on bar slip and bar extension (strain). Based on these results, use of the model detailed in ASCE 41-06 Supplement #1 is recommended, i.e., use a moment-curvature analysis to define the secant stiffness at the yield point and include a slip/extension spring. Alternatively, as noted in ASCE 41-06 (2007), the effective bending stiffness can be defined to provide an equivalent stiffness that combines both curvature and slip deformations.

Table 3. Summary of effective secant stiffness at yield for various code-prescribed methods compared to test results.

	Test Results	FEMA 356	ASCE 41	ASCE 41 S1, w/slip hinge	NZS-3101 95 ($\mu=1$)
$EI_{eff} [\% EI_g]$	14.0 12.5*	50.0	30.0	16.5 13.0*	50.0
$\theta_y [\% drift]$	0.70 1.00*	0.23	0.39	0.75 0.95*	0.23

*Modifications for 1/2-scale

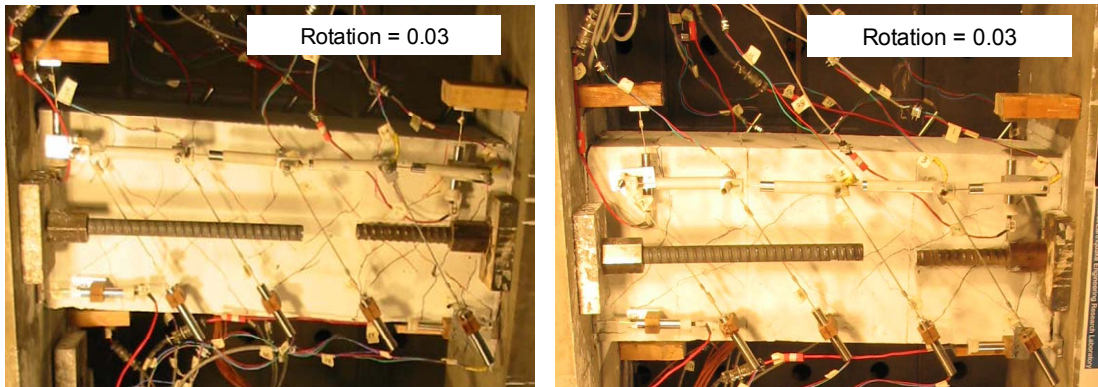


Figure 6. Photographs of beam damage at 3% rotation: (a) CB24F, and (b) CB24D.

As previously stated, the tests were conducted at one-half scale; therefore, it is important to understand the potential impact of scale on the effective yield stiffness as well as the overall load-deformation behavior. The relative contribution of flexural deformations (curvature) and slip/extension to the yield rotation of the test beams at full scale (i.e. prototype beams) is assessed using the same approach as noted in the previous paragraph for the one-half scale beams. The study is extended to consider coupling beam aspect ratios beyond those tested, by varying the beam length. Results are reported in Fig. 7, where the effective yield rotation is plotted against beam aspect ratio (l_n/h) for various scale factors. For a given aspect ratio, slip rotation at yield is significantly impacted by scale, with a 35 to 40% reduction for beams at one-half versus full scale. The effective bending stiffness at yield for the one-half scale tests of $0.12 E_c I_g$ increases to $0.14 E_c I_g$ for the full-scale prototypes due to the reduction in the relative contribution of slip rotation.

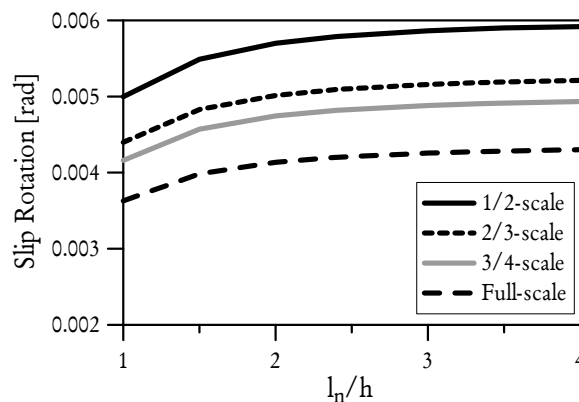


Figure 7. Yield rotation due to slip/extension for various aspect ratios and testing scales.

Linearized backbone relations for normalized shear strength versus rotation are plotted in Fig. 8 as dotted lines for the three configurations of beams tested. The backbone relations that are modified to represent full-scale beams are also plotted in Fig. 8, as discussed in the prior subsection. For configurations with multiple tests, an average relation is plotted. Backbone relations modified to represent full-scale beams indicate that the total rotations at yield, strength degradation, and residual strength are reduced to 0.70%, 6.0%, and 9.0%, respectively (from 1.0%, 8.0%, and 12.0%). ASCE 41-06 with Supplement #1 modeling parameters also are plotted on Fig. 8. Relative to ASCE 41-06, the relations derived for the full-scale beams have a lower effective yield stiffness ($0.14E_cI_g/0.3E_cI_g = 0.47$) and substantially greater deformation capacity ($5.3\%/3.0\% = 1.77$). It is reasonable to use a plastic rotation value of 5.0% with no strength degradation, with moderate residual strength ($0.3V_n$) up to a plastic rotation of 7.0%, compared to the ASCE 41-06 residual strength ratio of 0.8 at a plastic rotation value of 5.0%. It is noted that the ASCE 41-06 relation applies to all diagonally-reinforced coupling beams, including beams with aspect ratios significantly less than the values of 2.4 and 3.33 investigated in this test program. Results presented in Fig. 8 apply for the beam aspect ratios tested (2.4 and 3.33), as well as to beams between these ratios. It is reasonable to assume these values can be extrapolated modestly to apply to beams with $2.0 < l_n/h < 4.0$.

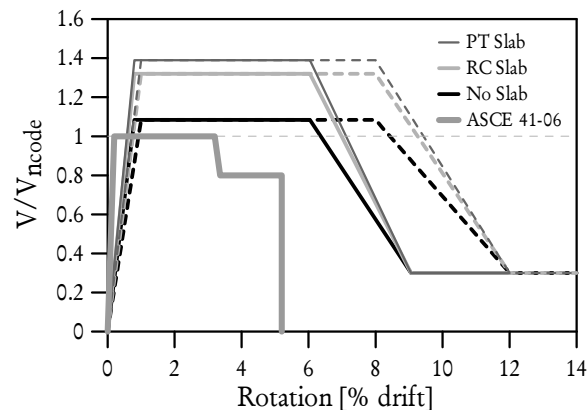


Figure 8. Backbone load-deformation for full-scale beam models and ASCE 41-06 model (1/2-scale test results are dotted lines).

Based on the backbone and effective stiffness relations discussed above, nonlinear modeling approaches commonly used by practicing engineers were investigated to assess how well they were able to represent the measured test results. Two models were considered, one utilizing a rotational spring at the ends of the beam to account for both nonlinear flexural and slip/extension deformations (M_n hinge) and one utilizing a nonlinear shear spring at beam mid-span to account for both shear and slip/extension deformations (V_n hinge). The M_n -hinge model consists of an elastic beam cross-section with $E_cI_{eff} = 0.5E_cI_g$, elastic-rotation springs (hinges) at each beam-end to simulate the effects of slip/extension deformations, and rigid plastic rotational springs (hinges) at each beam-end to simulate the effects of nonlinear deformations. The stiffness of the slip/extension hinges were defined using the Alsiwat and Saatcioglu model discussed above, whereas the nonlinear flexural hinges are modeled using the backbone relations derived from test results (Fig. 7, excluding the elastic portion). The V_n -hinge model also consists of an elastic beam cross-section and slip/extension hinges. However, instead of using flexural

hinges at the beam ends, a shear force versus displacement hinge (spring) is used at the beam mid-span to simulate the effects of nonlinear deformations. The shear hinge properties are defined using the backbone relations derived from the test results (Fig. 8).

Fig. 9 shows cyclic load-deformation plots for the two models and the test results for CB24F. Both models accurately capture the overall load-displacement response of the member; however, the M_n -hinge model (Fig. 9a) captures the unloading characteristics better than the V_n -hinge model (Fig. 9b), due to the fact that unloading stiffness modeling parameters, which help to adjust the slope of the unloading curve, are available for the flexural hinges in the commercial computer program used, but not for the shear hinges. Therefore, depending on the computer program used, similar modeling studies should be conducted to calibrate available model parameters with test results.

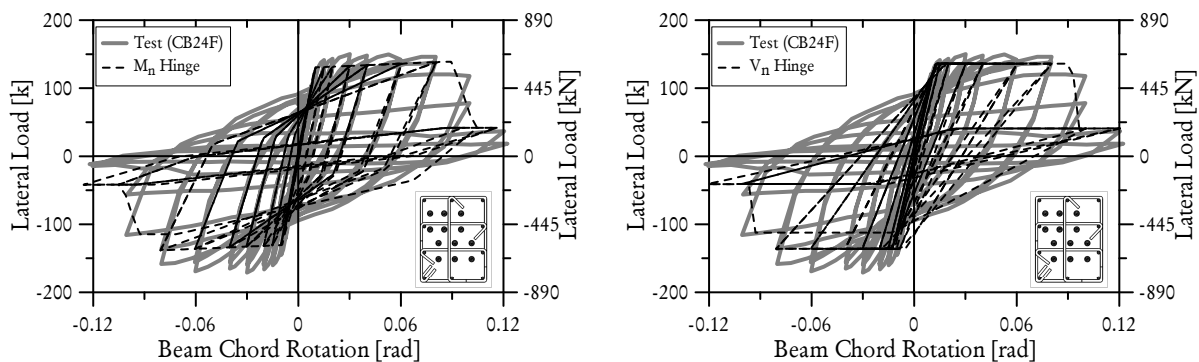


Figure 9. Cyclic load-deformation modeling results ($l_n/h = 2.4$): (a) CB24F vs. moment hinge model; and (b) CB24F vs. shear hinge model.

Conclusions

Beams detailed according to the new provision in ACI 318-08, which allows for full section confinement, have performance, in terms of strength and ductility, that is better than beams detailed according to the old provision in ACI 318-05, which requires confinement of the diagonal bar groups. Including a reinforced concrete slab increases the beam shear strength approximately 15-20%, with the strength increase directly related to the increase in beam moment strength, as the beam shear force was limited by flexural yielding. Beams detailed to satisfy $1/2 A_{sh}$ perform well at chord rotations $\theta < 3.0\%$. However, at very large rotations ($\theta > 6.0\%$), the beams experienced greater levels of damage compared with beams detailed to satisfy A_{sh} . The results indicate that the amount of transverse reinforcement required could be modestly reduced for the beam aspect ratios tested, especially for beams with lower ductility requirements ($\theta < 3.0\%$). However, further study is necessary.

Effective elastic stiffness values for test beams are determined to be $\sim 15\%$ of the gross section stiffness, values that are much less than FEMA and ASCE 41 prescribed values of 50% and 30%, respectively. Designers should therefore utilize the slip/extension hinge model detailed in Supplement 1 to ASCE 41 to better approximate the elastic stiffness of the coupling beam. Simple nonlinear models, either moment-hinge or shear-hinge, accurately represent the load-deformation behavior of test beams. The flexural hinge model better matches the test results in

the unloading and reloading range, due to the specific modeling parameters available in the computer software used (unloading stiffness modeling parameters), although both models produce acceptable results up to 3% total rotation for beams with l_n/h between 2.0 and 4.0.

Acknowledgments

The research has been funded by the Charles Pankow Foundation, with significant in-kind support provided by Webcor Concrete.

References

- ACI Committee 318, 1995, 2005, 2008, *Building Code Requirements for Structural Concrete (ACI 318-95/05/08) and Commentary (318R-95/05/08)*, American Concrete Institute, Farmington Hills, Michigan.
- Alsawat, J., and Saatcioglu, M., 1992. Reinforcement Anchorage Slip under Monotonic Loading, *Journal of Structural Engineering*, ASCE, Vol. 118, No. 9, pp. 2421-2438.
- American Society of Civil Engineers, 2007, *ASCE/SEI Standard 41-06, Seismic Rehabilitation of Existing Buildings*, Reston, VA.
- Elwood, K.J., et al., 2007, Update to ASCE/SEI 41 Concrete Provisions, *Earthquake Spectra*, EERI, Vol. 23, Issue 3, pp. 493-523.
- Federal Emergency Management Agency, 2000, *Prestandard and Commentary for the Seismic Rehabilitation of Buildings (FEMA-356)*, Washington DC.
- Galano, L., and Vignoli, A., 2000, Seismic Behavior of Short Coupling Beams with Different Reinforcement Layouts, *ACI Structural Journal*, V. 97, No. 6, Nov.-Dec., pp. 876-885.
- Naish, D., Fry, A., Klemencic, R., and Wallace, J., 2009, Experimental Evaluation and Analytical Modeling of ACI 318-05/08 Reinforced Concrete Coupling Beams Subjected to Reversed Cyclic Loading, *UCLA-SGEL Report 2009/06*.
- New Zealand Standards Association (NZS), 1995, *NZS 3101:1995 Concrete Structures Standard*, Wellington, New Zealand, 256 pp.
- Paulay, T., and Binney, J. R., 1974, Diagonally Reinforced Coupling Beams of Shear Walls, *Shear in Reinforced Concrete, SP-42*, American Concrete Institute, Farmington Hills, Mich., pp. 579-598.
- Tassios, T. P.; Moretti, M.; and Bezas, A., 1996, On the Coupling Behavior and Ductility of Reinforced Concrete Coupling Beams of Shear Walls, *ACI Structural Journal*, V. 93, No. 6, Nov.-Dec., pp. 711-720.
- Wallace, J. W., 2007, Modeling issues for tall reinforced core wall buildings, *The Structural Design of Tall and Special Buildings*, V. 16, No. 5, pp. 615-632.